

Discovery of two distinct red clumps in NGC 419: a rare snapshot of a cluster at the onset of degeneracy

Léo Girardi¹, Stefano Rubele^{1,2} and Leandro Kerber³

¹ Osservatorio Astronomico di Padova – INAF, Vicolo dell’Osservatorio 5, I-35122 Padova, Italy

² Dipartimento di Astronomia, Università di Padova, Vicolo dell’Osservatorio 2, I-35122 Padova, Italy

³ Universidade de São Paulo, IAG, Rua do Matão 1226, Cidade Universitária, São Paulo 05508-900, Brazil

To appear in MNRAS Letters (www.blackwell-synergy.com). Accepted 2008 Dec. 10. Received 2008 Dec. 9; in original form 2008 Nov. 14

ABSTRACT

Colour–magnitude diagrams (CMD) of the SMC star cluster NGC 419, derived from HST/ACS data, reveal a well-delineated secondary clump located below the classical compact red clump typical of intermediate-age populations. We demonstrate that this feature belongs to the cluster itself, rather than to the underlying SMC field. Then, we use synthetic CMDs to show that it corresponds very well to the secondary clump predicted to appear as a result of He-ignition in stars just massive enough to avoid e^- -degeneracy settling in their H-exhausted cores. The main red clump instead is made of the slightly less massive stars which passed through e^- -degeneracy and ignited He at the tip of the RGB. In other words, NGC 419 is the rare snapshot of a cluster while undergoing the fast transition from classical to degenerate H-exhausted cores. At this particular moment of a cluster’s life, the colour distance between the main sequence turn-off and the red clump(s) depends sensitively on the amount of convective core overshooting, Λ_c . By coupling measurements of this colour separation with fits to the red clump morphology, we are able to estimate simultaneously the cluster mean age ($1.35_{-0.04}^{+0.11}$ Gyr) and overshooting efficiency ($\Lambda_c = 0.47_{-0.04}^{+0.14}$). Therefore, clusters like NGC 419 may constitute important marks in the age scale of intermediate-age populations. After eye inspection of other CMDs derived from HST/ACS data, we suggest that the same secondary clump may also be present in the LMC clusters NGC 1751, 1783, 1806, 1846, 1852, and 1917.

Key words: Stars: evolution – Hertzsprung-Russell (HR) and C-M diagrams

1 INTRODUCTION

In the last decade, wide field imagers and the Hubble Space Telescope (HST) have provided detailed CMDs for the star fields in the Magellanic Clouds. One of the main surprises was the discovery that the red clump of core-He burners is not a compact feature, but may present extensions amounting to a few 0.1 mag departing from its top and bottom parts, as well as a blue extension that connects with the horizontal branch of the old metal-poor populations.

The ground-based observations from Bica et al. (1998) and Piatti et al. (1999) evinced a ~ 0.4 mag extension of the red clump to fainter magnitudes, spread over wide areas of the outer LMC disk. Girardi (1999) gave a clear interpretation to this extension – thereafter named *secondary red clump* – claiming that it is made of the stars just massive enough to start burning He in non-degenerate conditions, at ages of ~ 1 Gyr, whereas the main body of the red clump is made of all the intermediate-age and old stars which passed through degenerate cores and the He-core flash at the tip of the RGB. The same feature was suggested to be present in the Hipparcos CMD for the Solar Neighbourhood (Girardi et al. 1998), and provides an explanation to the vertical extension – amounting to about 0.8 mag in the $F814W$ band (see e.g. Holtzman et al. 1997)

– of the red clump in the sharp CMDs obtained by the HST for several LMC fields.

Plots of the red clump magnitude versus age for star clusters – as in Girardi (1999, figs. 3 and 4), and Grocholski & Sarajedini (2002, fig. 6) – seem to confirm the theoretical framework that led to Girardi’s (1999) prediction of a secondary clump: they clearly indicate a red clump decreasing in luminosity up to ~ 1 Gyr, then a jump upwards by about 0.4 mag, and a much slower evolution thereafter.

A handful of faint red clump stars are also found among the radial velocity members of the open clusters NGC 752 and 7789, and possibly also in NGC 2660 and 2204 (Mermilliod et al. 1998; Girardi et al. 2000). The latter authors associated these stars with the secondary clump feature, and tried to figure out how it could appear in an object for which the age spread was supposedly very small. Indeed, from their discussion it is clear that a single cluster age corresponds to a very narrow range of red clump masses and hence to the sampling of either the faint (secondary) or the bright (classical) red clump. The two red clumps could not appear together in a single star cluster, unless some other mechanism – e.g.

a dispersion in the mass loss along the RGB, or in the efficiency of overshooting on the main sequence (MS) – were invoked.

The reasoning from Girardi et al. (2000) would however now fail, at least for the star clusters in the Magellanic Clouds. Indeed, now *we know* that many of them do not represent single ages, but rather a range of ages that can extend up to a few 100 Myr (Mackey et al. 2008; Milone et al. 2008) – or equivalently, to a range of MS turn-off (MSTO) masses of a few $0.05 M_{\odot}$.

By visual inspection of the CMDs for a few SMC star clusters studied by Glatt et al. (2008), we came across what was *very evidently* a composite structure of main+secondary red clump in NGC 419. The presence of a secondary clump in this cluster was indeed noticed by Glatt et al. (2008, their sect. 3.6), who however have suggested it to be “a red clump of the old SMC field star population”. They also noticed the composite structure in the MS, attributing it to an extended period of star formation, similarly to the one claimed by Mackey et al. (2008) for three LMC clusters.

In the following, we demonstrate that the composite structure of the red clump in NGC 419 is real and undubiously associated to the cluster (Sect. 2). We show that it corresponds to the simultaneous presence of stars which have started burning He under non-degenerate and degenerate conditions (Sect. 3). We then illustrate that this rare occurrence in a cluster allows us to set stringent constraints on the cluster age and amount of convective core overshooting during the MS evolution (Sect. 4). We then briefly suggest that NGC 419 is not a unique case, and draw some final comments in Sect. 5.

2 NGC 419 PHOTOMETRY AND CMD

We have retrieved from the HST archive the NGC 419 data obtained by GO-10396 (PI: J.S. Gallagher). The dataset consists of a 740 arcsec^2 area observed with the Advanced Camera for Surveys (ACS) High Resolution Channel (HRC) centered on NGC 419, plus a $4.24 \times 10^4 \text{ arcsec}^2$ area observed with the ACS Wide Field Channel (WFC) $37''$ offset from the cluster centre. Both datasets were reduced via standard procedures (Sirianni et al. 2005). The HRC data, given its high spatial resolution, is the most useful for the study of the NGC 419 population, whereas the WFC dataset provides the comparison data for interpreting the SMC field.

We have performed aperture and PSF photometry on the calibrated HRC image, finding that both provide CMDs very similar to the Glatt et al. (2008) ones. We have then opted for the PSF catalogue and cutted it at $(\text{sharp}_{F555W}^2 + \text{sharp}_{F814W}^2)^{1/2} < 0.2$. This quality cut eliminates many outliers from the CMD, especially at the faintest magnitudes, but do not affect the morphology of features at the red clump and MSTO level.

The HRC data is plotted in Fig. 1, which shows both the global CMD and separate panels detailing the red clump and the MSTO regions. The extended nature of the red clump is evident in the figure¹. It seems to be formed by a main blob located between $F814W = 18.1$ and 18.65 , followed by a well-defined faint wing between $F814W = 18.65$ and 19.0 , which we tentatively identify as the secondary clump. We note that there is no similar wing extending from the top of the red clump. These sequences are about

¹ The choice of the $F814W$ band for the ordinate is not casual, since $F814W$ presents flatter bolometric corrections than $F555W$, over the T_{eff} range of the red clump. This improves the separation in magnitude of the clump substructures, and at the same time keeps the subgiant branch out of its magnitude range.

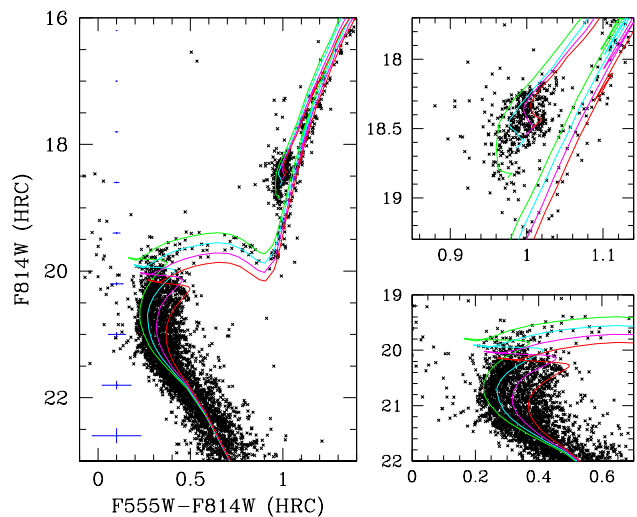


Figure 1. The CMD for NGC 419 as derived from the HRC data centered on the cluster (left panel). The 1σ error bars, as derived from artificial star tests, are drawn at the left. The right panels detail the red clump (top) and MSTO regions (bottom). The overlaid isochrones are from Marigo et al. (2008), for a metallicity $Z = 0.004$, ages varying from $\log(t/\text{yr}) = 9.10$ to 9.25 with a constant spacing of 0.05 dex, $E_{F555W-F814W} = 0.09$, and $(m-M)_{F814W} = 18.85$. Notice that these particular isochrones describe reverse sequences in the MSTO and red clump regions of the CMD: whereas the MSTO gets dimmer for increasing ages, the red clump gets brighter.

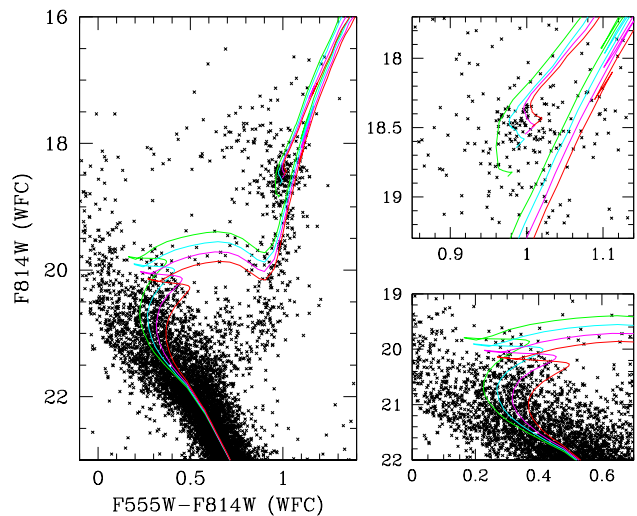


Figure 2. The CMDs for $2.47 \times 10^4 \text{ arcsec}^2$ field around NGC 419, as derived from the WFC data after subtracting a circular area of radius $75''$ around the cluster. The overlaid isochrones are the same as in Fig. 1, and are plotted for reference only. The bulk of the red clump is below the saturation limit at $F555W \sim 17.9$.

0.08 mag bluer (in $F555W - F814W$) than the ridgeline of RGB stars. In addition, the red part of the CMD shows a well delineated subgiant branch, and the bump of early asymptotic giant branch (AGB) stars centered at $F814W = 17.7$.

There are 55 stars between $F814W = 18.65$ and 19.0 , 8 out of which are red enough to belong to the RGB rather than to the secondary clump. The main red clump instead contains 341 stars. These numbers correspond to the HRC effective area of 740 arcsec^2 , centered on NGC 419. We verified that both sets of

stars distribute all over the HRC image, and share similar distributions of photometric errors and sharpness. So, it is unlikely that the secondary clump could be an artifact of a given subsample of the data.

Can the field SMC stars account for the 47 stars in the secondary clump, as suggested by Glatt et al. (2008)? To answer this question, we look at the WFC data of Fig. 2, which covers an area 33 times larger than the HRC one. It was obtained subtracting from the complete WFC catalogue – without applying any quality cut – a circular area of $75''$ in radius around NGC 419. The remaining area of 2.47×10^4 arcsec² was considered to be “SMC field”, and contains 150 red clump stars in the $F814W$ range between 18.1 and 19.0. Therefore, the expected number of these stars in the 740 arcsec² area of HRC is of just 4.5. Moreover, their typical magnitudes are closer to those of the main red clump in NGC 419, rather than to the secondary one. We conclude that the field cannot contribute with more than $\sim 10\%$ of the 47 stars observed in the secondary clump, and probably contribute much less. *The bulk of the secondary clump observed in HRC data indeed belongs to NGC 419.*

3 MODELLING THE TWO CLUMPS

Our interpretation of the red clump structure in NGC 419 is already clear in Fig. 1 and in the discussion of Sect. 1: the fainter secondary red clump is explained by the core-He burning stars belonging to the younger isochrones, which have just avoided e^- -degeneracy before igniting He. This feature has been thoroughly discussed in Girardi (1999) and Girardi et al. (1998), in the context of galaxy field populations. It appears naturally in simulations of star-forming galaxies with moderate-to-high metallicities, provided that the underlying stellar models do present a fine resolution in mass (better than $0.1 M_\odot$; see Girardi 1999).

In the following, we discuss the specific case of NGC 419 by means of newly-computed evolutionary tracks of initial composition ($Z = 0.004$, $Y = 0.250$). The input physics is the same as in Bertelli et al. (2008). We have initially adopted a moderate amount of convective overshooting, i.e. $\Lambda_c = 0.5$, where Λ_c is the size of the overshooting region across the convective boundary, in pressure scale heights, following the Bressan et al. (1981, 1993) definitions. For a limited interval of initial masses M_i , typically going from $M_{\text{HeF}} - 0.4 M_\odot$ to $M_{\text{HeF}} + 0.4 M_\odot$, we follow the evolution up to the thermally pulsing AGB, whereas for smaller masses (down to $0.6 M_\odot$) we have computed only the MS evolution. Stellar tracks are spaced by $\Delta M_i = 0.05 M_\odot$. These tracks are converted to stellar isochrones in the ACS/HRC and ACS/WFC Vegamag systems using the transformations from Girardi et al. (2008).

The isochrones are then fed to the TRILEGAL population synthesis code (Girardi et al. 2005) to simulate the photometry of star clusters at the SMC distance. We apply to the TRILEGAL output the photometric errors derived from artificial star tests performed on the original HRC images. The results are illustrated in Fig. 3, which shows the expected time evolution of the red clump for a cluster for two different cases: either for an almost-instantaneous burst of star formation (with a duration of $\Delta \log t = 0.01$), and for a burst spanning a range of $\Delta \log t = 0.15$. The latter case corresponds roughly to the situation indicated by the MSTO stars in Fig. 1. 20 % of the stars in the simulation are assumed to be detached binaries with a mass ratio comprised between 0.7 and 1 (Woo et al. 2003). Since this latter prescription is rather uncertain, binaries are always marked with a different colour in our plots.

It is evident from Fig. 3 that the red clump rapidly transits from a vertically-extended feature, to a much more compact and slightly brighter clump at a mean age t close to 1.25 Gyr. The transition takes place completely in an age interval of just ~ 0.1 Gyr for the case of an instantaneous burst, and in about twice this time for the case of a $\Delta \log t = 0.15$ -wide burst. From now on, we will refer to the mean age of this transition as t_{HeF} .

We note that vertically-extended red clumps are present for all ages younger than t_{HeF} , even in the instantaneous-burst case; however, they are wider than observed in NGC 419, and present drop-shaped LFs – i.e. with a sharp cut at the bottom and a more extended tail at the top. This is not what observed in the red clump of NGC 419, which presents the maximum of its LF at the top, together with a bump at the faintest magnitudes. A configuration similar to NGC 419 is obtained only in the extended-burst case, for ages comprised between 1.41 and 1.58 Gyr: indeed, this age range is the only one which combines the vertically-extended red clump of younger ages, with the compact and brighter red clump of older ages, in about the right proportions to explain the observations. We identify NGC 419 as belonging to this very limited – and surely very singular – age interval. In order to identify the best-fitting age, we compute the χ^2 between data and model, for the red clump region only. The distance modulus is varied until the minimum value of χ^2 is met for each age t . The results are printed in Fig. 3, and evince the excellent quality of the fit for the 1.41 Gyr-old model with $\Delta \log t = 0.15$.

Finally, it is worth mentioning that the MS+red clump binaries tend to draw a plume departing from the red clump towards bluer colours and brighter magnitudes, which (1) is easily identifiable in observed CMDs because of its colour separation from the red clump, and (2) do not change the drop-shaped form of the LF for the younger red clumps. Binaries cannot mimick the bimodal LF observed in the red clump of NGC 419.

A question raised by the referee is whether the two red clumps could be caused by populations with different helium content, abundances of CNO elements, or overshooting efficiency. Although nothing can be excluded, so far there are no indications of such effects in clusters as young as NGC 419. Moreover, it is Occam’s razor to refrain us from looking for more complicate alternatives: in fact, our explanation requires *only* standard physics added to a quite simple distribution of stellar ages – the same one indicated by the clusters’ MSTO – while keeping all other parameters constant. We recall that the transition between faint and bright red clump is something that inevitably happens, sooner or later, for *every* single stellar population, causing *always* about the same amount of brightening in the red clump over a similar timescale (which is dictated mainly by the equation of state of partially-degenerate matter). Therefore, there is no free parameter to be fixed in order to explain the presence and position of the two red clumps, there is just the very loose requirement of “a prolonged-enough duration of the star formation”.

4 OVERSHOOTING AND THE AGE SCALE

According to the interpretation given in this letter, the red clump in NGC 419 corresponds to stars with a precise internal configuration after H-exhaustion: their cores have a mass very close to $0.33 M_\odot$, as their central temperatures approach $T_c = 10^8$ K. Slightly higher core masses lead to non-degenerate He-ignition. Slightly smaller core masses lead to e^- -degeneracy, which halts the core contraction and is followed by the cooling of the central core by plasma

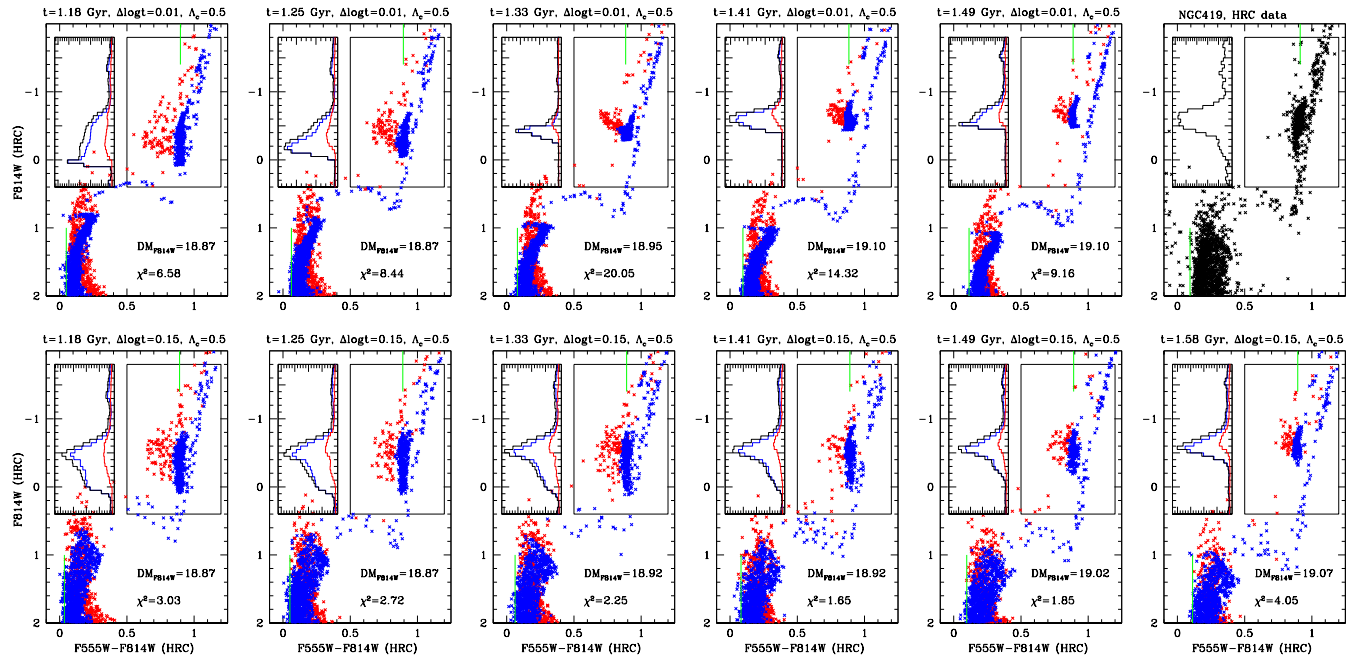


Figure 3. Models for the evolution of the red clump feature in the CMD as a function of mean population age t , for both a single-burst population (top panels) and for a composite one with duration of $\Delta \log t = 0.15$ (bottom panels), in both cases with the assumption of moderate convective overshooting ($\Lambda_c = 0.5$) and $Z = 0.004$. Single stars are marked in blue, double stars in red. Each panel presents on the top right a box evincing the red clump, and on the top left the luminosity function (LF) for the stars in this box. The best-fitting distance modulus and the associated χ^2 are also displayed. For comparison, the top right panel shows the HRC data of NGC 419 on the same scale, after being arbitrarily shifted by 19.0 and 0.09 in magnitude and colour, respectively. The green vertical lines in all panels mark the median colour of the red clump, and the bluest colour of the MS (see text).

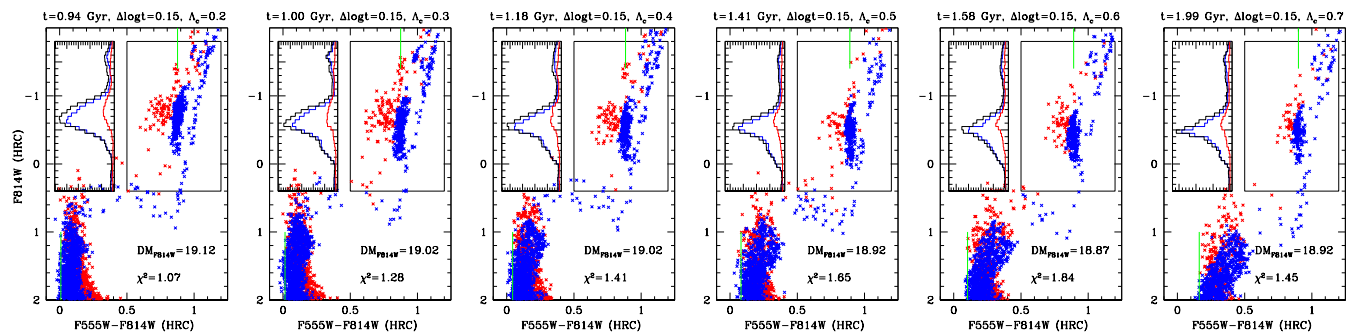


Figure 4. Top panels: The same as in Fig. 3, but now showing the models that best fit the red clump for several values of overshooting efficiency Λ_c , and for the $\Delta \log t = 0.15$ case only. Although all models reproduce the observed red clump similarly well, they differ very much in their age (from 0.94 to 1.99 Gyr, as Λ_c increases from 0.2 to 0.7), and produce different MSTO magnitudes and colours.

neutrinos; as a consequence the He-ignition is postponed to a later stage – namely the RGB tip – at which the core masses have grown up to $0.45 M_{\odot}$ (see Sweigart et al. 1990).

These core masses after H-exhaustion do also correspond to a narrow interval of initial masses, comprehending the transition between intermediate- and low-mass stars, M_{HeF} . It has long been known that convective core overshooting changes the relation between the initial mass and the H-exhausted core mass, hence directly affecting the value of M_{HeF} , and its corresponding age t_{HeF} (e.g. Bressan et al. 1993). Even if the efficiency Λ_c can be constrained by means of several methods which use either the morphology of the CMD or star count ratios (e.g. Woo et al. 2003, and references therein), this is still a main source of uncertainty in settling the age scale of intermediate-age clusters, and in the theory of stellar populations in general.

Can the NGC 419 giants help us to set constraints on M_{HeF}

and t_{HeF} , and hence on Λ_c ? Probably yes, considering that higher M_{HeF} values (lower Λ_c) imply bluer MSTOs. Once we identify a star cluster during the particular age t_{HeF} , fixing the position of its red clump(s) in the CMD, the relative position of the MSTO should depend mainly on overshooting.

With this idea in mind, we have computed several set of stellar evolutionary tracks and isochrones, with Λ_c varying from 0.2 to 0.7. For each one of these sets we identify the age at which, for a $\Delta \log t = 0.15$ star formation burst, the red clump morphology is best reproduced (just as in Fig. 3). Indeed, Fig. 4 shows that similarly good fits of the red clump morphology are obtained for all values of Λ_c , but at different ages t_{HeF} . We recall that these different fits actually represent *very similar distributions of the core mass after H-exhaustion*.

We then measure the colour difference between the median of the red clump, and the bluest border of the MSTO region de-

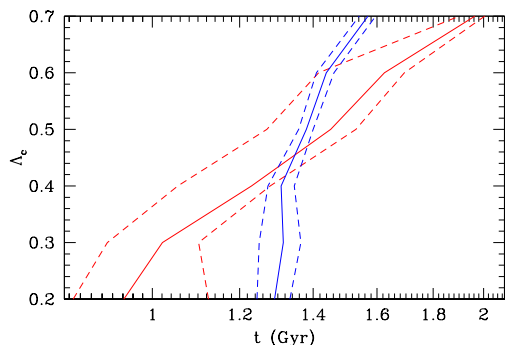


Figure 5. Confidence regions in the t vs. Λ_c plane. The continuous red line follow the locus of minimum χ^2 values derived from the fitting of the red clump morphology (see also Fig. 4). The continuous blue line describe the models which perfectly fit the colour difference between the red clump and MSTO. Dashed lines present the estimated 70% confidence limits.

finied by the 98% percentile of the star counts above an absolute magnitude of 2.5. This quantity is little sensitive to the fraction of binaries, and our simulations indicate that it can be measured with a 1σ error of 0.006 mag. Fig. 5 shows this quantity in the t vs. Λ_c plane, together with the estimated 70% confidence level region of the best-fitting model to the red clump morphology. The best simultaneous fit of the two quantities is obtained for $\Lambda_c = 0.47_{-0.04}^{+0.14}$ and $t = 1.35_{-0.04}^{+0.11}$ Gyr (with random errors only).

Importantly, these t and Λ_c determinations are largely free from uncertainties in the cluster distance and reddening. However, they may be slightly affected by other factors like the assumed fraction of binaries, the mixing-length parameter, and the detailed star formation history of NGC 419. More detailed analysis (in preparation) will aim to reduce these uncertainties by using information from the complete CMD, and better exploring the parameter space. A few preliminary conclusions can be advanced here: (1) Models for $\Delta \log t$ values of 0.1 and 0.2 do also provide good fits of the red clump morphology, with their best-fitting ages differing by less than 6% from those we find for $\Delta \log t = 0.15$; these age differences are comparable to the above-mentioned random errors. However, such models have to be excluded because they clearly provide a worst description of the MSTO region of the CMD. (2) On the other hand, models with a fraction of binaries as small as 10% tend to provide slightly better fits of the red clump LF, at essentially the same ages as those found with 20% of binaries, and with just a modest impact in the morphology of the MSTO.

5 FINAL CONSIDERATIONS

NGC 419 can be definitely added to the list of star clusters with a secondary red clump, together with the Milky Way open clusters NGC 752 and 7789, and possibly also NGC 2660 and 2204, which were already discussed by Girardi et al. (2000). This time, however, we are facing a very populous cluster which presents a CMD rich of details, from its lower MS up to the AGB carbon star sequence (see Fig. 1, and Frogel et al. 1990). The secondary red clump itself is very well populated and its detection can hardly be controversial. This fine CMD feature provides strong constraints to the core mass reached by its MS stars. All these aspects make of NGC 419 an excellent tool for calibrating stellar evolution models, as well as the age sequence of intermediate-age populations.

Can we identify additional star clusters in the Magellanic

Clouds, having the same secondary clump feature? Probably yes, since these galaxies contain dozens of populous clusters with ages around 1 Gyr, and the presence of multiple turn-offs is a common feature among them (Milone et al. 2008). Indeed, from a rapid eye inspection of published CMDs obtained with HST/ACS, we notice that dual (main+secondary) red clump structures seem to be present also in the LMC clusters NGC 1751, 1783, 1806, 1846, 1852, and 1917 – see figs. 7, 8, 9, 16 and 17 in Milone et al. (2008), and fig. 1 in Mackey et al. (2008). All these clusters have multiple turn-offs, with the youngest one being at $F814W \sim 19.5$, which is comparable with the NGC 419 one if we consider the ~ 0.5 mag difference in the SMC–LMC distance moduli. A subsequent paper will examine these clusters in close detail, in the perspective of deriving more stringent constraints to stellar evolutionary models. Cluster fundamental parameters such as the age, distance and reddening, will be re-evaluated as well.

ACKNOWLEDGMENTS

The data presented in this paper were obtained from the Multi-mission Archive at the Space Telescope Science Institute (MAST). STScI is operated by the Association of Universities for Research in Astronomy, Inc., under NASA contract NAS5-26555. We thank A. Bressan, G. Bertelli and M. Clemens for the useful comments, and support from INAF/PRIN07 CRA 1.06.10.03, contract ASI-INAF I/016/07/0, and the Brazilian agencies CNPq and FAPESP.

REFERENCES

- Bertelli G., Girardi L., Marigo P., Nasi E., 2008, *A&A*, 484, 815
- Bica E., Geisler D., Dottori H., Clariá J. J., Piatti A. E., Santos Jr. J. F. C., 1998, *AJ*, 116, 723
- Bressan A., Fagotto F., Bertelli G., Chiosi C., 1993, *A&AS*, 100, 647
- Bressan A. G., Chiosi C., Bertelli G., 1981, *A&A*, 102, 25
- Frogel J. A., Mould J., Blanco V. M., 1990, *ApJ*, 352, 96
- Girardi L., 1999, *MNRAS*, 308, 818
- Girardi L., et al., 2008, *PASP*, 120, 583
- Girardi L., Groenewegen M. A. T., Hatziminaoglou E., da Costa L., 2005, *A&A*, 436, 895
- Girardi L., Groenewegen M. A. T., Weiss A., Salaris M., 1998, *MNRAS*, 301, 149
- Girardi L., Mermilliod J.-C., Carraro G., 2000, *A&A*, 354, 892
- Glatt K., et al., 2008, *AJ*, 136, 1703
- Grocholski A. J., Sarajedini A., 2002, *AJ*, 123, 1603
- Holtzman J. A., et al., 1997, *AJ*, 113, 656
- Mackey A. D., Broby Nielsen P., Ferguson A. M. N., Richardson J. C., 2008, *ApJ*, 681, L17
- Marigo P., Girardi L., Bressan A., Groenewegen M. A. T., Silva L., Granato G. L., 2008, *A&A*, 482, 883
- Mermilliod J.-C., Mathieu R. D., Latham D. W., Mayor M., 1998, *A&A*, 339, 423
- Milone A. P., Bedin L. R., Piotto G., Anderson J., 2008, *arXiv:0810.2558*
- Piatti A. E., Geisler D., Bica E., Clariá J. J., Santos Jr. J. F. C., Sarajedini A., Dottori H., 1999, *AJ*, 118, 2865
- Sirianni M., et al., 2005, *PASP*, 117, 1049
- Sweigart A. V., Greggio L., Renzini A., 1990, *ApJ*, 364, 527
- Woo J.-H., Gallart C., Demarque P., Yi S., Zoccali M., 2003, *AJ*, 125, 754